Macromolecules

pubs.acs.org/Macromolecules Article

Restricted Orientation Anisotropy Method for FVE Radii Characterization: Confirmed and Refined via the Study of Six Vibrational Probes

Junkun Pan, Aaron P. Charnay, Sebastian M. Fica-Contreras, and Michael D. Fayer*

Cite This: https://doi.org/10.1021/acs.macromol.3c02093 Read Online

ACCESS | Metrics & More | Article Recommendations | Supporting Information

ABSTRACT: The Restricted Orientation Anisotropy Method (ROAM) is a new technique for determining polymer free volume element (FVE) radii using ultrafast infrared (IR) polarization-selective pump−probe (PSPP) spectroscopy. ROAM utilizes small IR vibrational probe molecules as molecular rulers to measure the FVE radii and the radius probability distribution (RPD). Here, we present a rigorous test of the method by performing ROAM experiments on polystyrene using six different probe molecules that have different lengths and shapes. In addition, we enhance the method for determining the length of the molecular ruler, resulting in greater accuracy. ROAM measures the orientational relaxation of the probes. Because the probes are too large to rotate in the FVEs completely, PSPP experiments provide their restricted angular ranges. The FVE radius is determined from the angular range and probe length. The IR measurements are made on the CN stretches of phenyl selenocyanate, phenyl thiocyanate, and four *para*-substituted benzonitriles (*p*-XBZN, where X = F, Cl, Br, I). The FVE radius measured using the six probes is the same with a small experimental error. The average of the radii measured at the spectral peaks of the six probes is 2.81 ± 0.02 Å. The RPD is determined and used to obtain the average radius, 2.94 Å, within a few hundredths of an Angstrom to values found with positron annihilation lifetime spectroscopy. The fact that six probes with different lengths and shapes give the same radius proves ROAM's efficacy and confirms the model of the FVEs as cylinders on the probe's length scale.

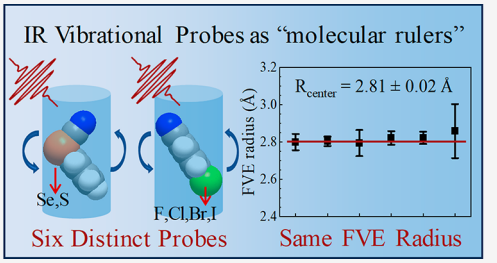

1. INTRODUCTION

Polymer research has been incredibly active since Leo Baekeland produced the first fully synthetic plastic, Bakelite,[1] in 1907. Polymers are important because of their synthetic tunability, low cost, and diverse applications.[2] Despite the general interest in the area and the vast amount of research conducted, a detailed understanding of structure−property relationships remains an active area of investigation because of the need for effective property predictions.[3] A great deal of successful research has focused on improving bulk properties for practical applications without studies of molecular-level properties and relationships.[4,5]

A fundamental property of amorphous polymers is free volume, defined as the difference between the total and hard sphere volumes.[6] Small-molecule liquids and glasses have free volume because their shapes are not space-filling. Polymers have this type of free volume, but they also have free volume elements (FVEs), which are relatively large voids with radii of a few angstroms,[7] that arise from the imperfect packing of polymer chains and only represent a small percentage of the total free volume. FVEs have been correlated to many important polymer properties. FVEs have been considered to participate in gas diffusion through the polymer membranes, which occurs via gas molecules moving through a polymer matrix from one FVE to another.[8−13] FVE characteristics have also been shown to be important for application in dielectric materials.[14−16] Recently, dielectric breakdown strengths have been correlated to the shapes of FVE radii probability distributions,[16] in accord with the breakdown theory of Artbauer.[17] Other macroscopic properties that FVEs have been proposed to influence are the glass-transition temperature (T_g),[18] physical aging,[19,20] and lithium transport in polymer electrolytes.[21,22] In addition, measurements of the average FVE size and the FVE size distribution for a particular polymer matrix can provide insights into chain packing.

Due to the complicated amorphous nature of glassy polymers and the small physical size of the FVEs, the quantitative characterizations of the FVE sizes and radius probability distributions have proven difficult.[23] Only a small number of experimental techniques have been used to make measurements of polymer FVEs, such as ^{129}Xe NMR,[24−26] inverse gas chromatography (IGC),[27] and positronium annihilation lifetime spectroscopy (PALS).[23,28−30] PALS has

Received: October 12, 2023
Revised: January 5, 2024
Accepted: January 9, 2024

been applied to study many different polymeric systems and has substantial efficacy for determining FVE sizes and, in some instances, size distributions.[31−33] PALS utilizes the *ortho*positronium (*o*-Ps) lifetime, which becomes shorter when the positronium wave function overlaps with the electron cloud of FVE walls.[31] Smaller FVEs give rise to more overlaps, resulting in shorter lifetimes. For the conversion of *o*-Ps lifetimes to radii, the semiempirical Tao−Eldrup equation,[34,35] which assumes a spherical FVE shape and a particle in a spherical box *o*-Ps wave function, is widely used. Although it has been argued that other shapes, such as cylindrical[25,36,37] and ellipsoidal,[38] may be better representations of FVEs, these models have not been generally adopted. The Tao−Eldrup equation was calibrated by applying PALS to a variety of materials, e.g., liquids[39,40] and zeolites,[41] in which various experimental methods were used to determine the radius of special cavities modeled as spheres. Although the calibration is not performed using polymers, the calibration curve of radius vs *o*-Ps lifetime is used to determine polymer FVE radii. The same FVE surface electron density is assumed for all polymers, independent of their chemical structure. The PALS results cannot be intrinsically tested in polymers, as the properties of *o*-Ps cannot be varied.

Recently, a new method, the restricted orientational anisotropy method (ROAM), was developed for the characterization of free volume elements using ultrafast infrared (IR) spectroscopy.[42,43] ROAM can determine the average FVE radius, the most probable radius, and the radius probability distributions (RPDs) as well as the average internal electric fields associated with a particular FVE radius.[43] ROAM employs IR vibrational probes as molecular rulers to report on the FVE sizes. IR polarization-selective pump−probe (PSPP) experiments are used to measure the range of angles (cone angles) that the vibrational probes sample via their orientational motions inside the FVEs. In a liquid, the probe would undergo complete orientational relaxation, i.e., sample all angles. However, because the FVE radii are small, the angular range sampled is restricted by the probe contacting the FVEs' walls. The angular range, called the cone angle, is extracted from the PSPP experiment. Obtaining the cone angles from the experimental measurements does not require assumptions. It is based on an established theory that was first developed in the 1970s and '80s[44−46] and used for a wide variety of experiments, such as fluorescence depolarization[47] and NMR.[48,49] The cone angle measured with PSPP experiments directly reflects the FVE size. For a given probe molecule, a larger FVE size will give a larger measured cone angle. Then, using the probe molecule's "molecular ruler" length, cone angles are converted into corresponding FVE radii.

Here, we put the ROAM technique to rigorous testing by studying six different probe molecules in polystyrene (PS). The probes have different molecular ruler lengths and molecular shapes. Nonetheless, all six probes yielded the same FVE radius within a small experimental error. The experiments are a rigorous test of ROAM, confirming its consistency in measuring FVE radii.

The vibrational probe used for previous ROAM experiments[16,42,43] was phenyl selenocyanate (PhSeCN). The PSPP experiments were performed on CN stretching mode. PhSeCN is a very useful probe because of its exceptionally long vibrational excited state lifetime (400 ps)[43,50] and its large Stark coupling constant (discussed in detail below). Both properties are useful for the acquisition of high-quality data. While PhSeCN's long lifetime and large Stark coupling constant make it valuable for ROAM experiments, its bent geometry requires careful consideration to determine the molecular ruler length correctly. Below, we show how to account for the molecular geometry by using the measured restricted orientational relaxation cone angles and the molecular ruler length to determine the FVEs' radii accurately. In addition, the PhSeCN probe has an internal rotational degree of freedom about the bond between the Se and the carbon on the phenyl ring to which it is bonded. The initial presentation of ROAM did not consider the influence of internal rotation. The influence of internal rotation was investigated, and it was shown that internal rotation does not interfere with the FVE radii measurement.

In the following tests, ROAM is shown to be correct and accurate by comparing experiments and analysis of the six different vibrational probes, PhSeCN, PhSCN, and four halogenated benzonitriles (*p*-XBZN, X = F, Cl, Br, I) all in PS. The different *para*-substituents on the benzonitrile probes allow us to study the effect of probe length systematically. The four *p*-XBZN probes do not have internal rotations or "bent" geometries, while PhSeCN and PhSCN do. The six probes measure different experimental cone angles, but when the appropriate molecular ruler length is determined and used, all probe molecules, with or without internal rotation, give the same FVE radius within a small error. Furthermore, the effects of the internal rotation barrier are examined by comparing PhSeCN and PhSCN. PhSCN has a smaller barrier for internal rotation than PhSeCN. The different barriers produced different time-dependent anisotropy decays but did not change the measured radii.

In light of the new experimental and theoretical results, we carefully account for different molecular geometries, improve the methodology for determining the molecular ruler lengths, and show how to accurately use the measured restricted orientational relaxation cone angles to determine the FVE radii. While the six probes give the same FVE radius, measured at the peak of each of their CN absorption spectra, to obtain the PS FVE radius probability distribution, it is necessary to have a large Stark coupling constant and a sufficiently long vibrational lifetime. PhSeCN has these characteristics and is used to obtain the RPD. Finally, the slow components of the PSPP decays are analyzed and discussed in terms of FVE surface topography fluctuations.

2. EXPERIMENTAL METHODS

2.1. Sample Preparation. The concentration of the probes in the polymer films is 300 mM. Previous probe concentration dependence studies showed that when the total concentrations of probes and solvents are below 500 mM (5%), decreasing the concentration does not affect the anisotropy.[43] However, during drying in a vacuum oven (see below), a significant amount of the probe diffuses out of the film. The final probe concentration was determined by NMR spectroscopy. The solvent concentrations for all samples were below 1%, and the remaining probe contents were below 2%. Therefore, the probe concentration did not affect the results of our measurements.

The sample preparation of the polystyrene films with embedded vibrational probes follows the procedures described in the previous publication.[43] Briefly, an appropriate amount of polystyrene was measured and dissolved in chloroform. For each sample, one of the vibrational probes (PhSeCN, PhSCN, *p*-FBZN, *p*-ClBZN, *p*-BrBZN, and *p*-IBZN) was also dissolved in the solution with a concentration so that the final polymer film has 300 mM probes. These solutions

https://doi.org/10.1021/acs.macromol.3c02093
Macromolecules XXXX, XXX, XXX−XXX

were poured into aluminum rings attached to a leveled flat glass plate. The top of the aluminum ring is partially covered to allow the solvent to evaporate slowly. Once the film solidifies, it is peeled from the glass substrate and transferred to a vacuum oven to remove the residual solvents. The samples are gradually heated to 90 °C and kept at that temperature for 5 days. The residual solvent content of each film is characterized by NMR spectroscopy. This procedure produces films with excellent optical quality with thicknesses of 250 ± 30 μm. Once the samples are removed from the vacuum oven, they are immediately transferred to a glovebox. A small piece of the film is cut from the sample and placed in an aluminum sample cell with CaF_2 widows for IR measurements.

It is worth noting that during the solvent removal process (drying) in a vacuum oven at temperatures below the glass-transition temperature, a significant amount of the probes, ∼50%, diffuses out of the ∼250 μm film. Because the amount of probe that is lost is substantial, it cannot be lost from just a thin layer near the surface. Therefore, when the ROAM measurements are made, the probe molecules move long distances from the locations they occupy at the end of the solvent-casting process.

2.2. NMR Characterization. ^{1}H NMR was used to quantify the films' residual solvent (chloroform) contents. Ten milligrams of a sample was cut from each film and dissolved in 750 μL of deuterated dichloromethane (DCM). The spectra were collected in a 400 MHz Varian NMR spectrometer by using VNMRJ 4.2 software. The complete details of the characterization and NMR spectra of the samples are presented in the Supporting Information (SI).

2.3. FTIR Measurements. FTIR spectra were measured using a Thermo Fisher iS50 infrared spectrometer with a resolution of 0.24 cm^{-1}. The absorption spectrum of the nitrile stretch of each vibrational probe in polystyrene was obtained by subtracting the background spectrum of pure polystyrene.

2.4. DFT Calculation. Geometry optimization of phenyl selenocyanate (PhSeCN), phenyl thiocyanate (PhSCN), and four halogenated benzonitriles (4-fluorobenzonitrile, 4-chlorobenzonitrile, 4-bromobenzonitrile, and 4-iodobenzonitrile) was performed using the Gaussian 16 quantum chemistry package[51] at the B3LYP/6-311++G(d,p) level of theory to determine the bond lengths and distances between different atoms. Additionally, PES calculations were performed for PhSeCN and PhSCN at the same level of theory for the dihedral C(Ph)-C(Ph)-Se/S−C(CN) from −90 to 90° with a step size of 5° to determine internal rotation barriers.

2.5. Polarization-Selective Pump Probe (PSPP) Experiment. A comprehensive description of the exact laser system used for the experiments has been provided previously.[42,43] Briefly, a regenerative amplifier seeded by a Ti:sapphire oscillator generated 800 nm femtosecond pulses (2 mJ, 3 kHz). The output from the regenerative amplifier is converted from 800 nm to 4.4−4.7 μm (30 μJ, 3 kHz) by a home-built optical parametric amplifier (OPA). The IR frequency was tuned to the absorption of the specific nitrile stretch frequency of the vibrational probe under investigation. The final mid-IR pulses have a bandwidth of ∼90 cm^{-1} and are near transform-limited.

The mid-IR pulse is split into a 90% intensity pump and a 5% intensity probe. The pump pulse passes through a germanium acousto-optic modulator (AOM) pulse shaping system, which provides arbitrary control of the pulses' phase and shape.[52] A mechanical delay stage controls the probe pulse's arrival relative to the pump pulse with a maximum time delay of ∼2 ns. The polarization of the pump pulse is set to +45° relative to probe polarization with a half-wave plate and a polarizer before the sample. A polarizer on a computer-controlled rotation stage is used after the sample stage to resolve the probe pulse at either +45° (parallel) or −45° (perpendicular). An additional horizontal polarizer is placed after the resolving polarizer to ensure the spectra with parallel and perpendicular polarizations have identical amplitudes. The probe pulses are frequency-resolved by a spectrograph and detected by a 32-pixel mercury cadmium telluride (MCT) array detector.

In a PSPP experiment, the pump pulse excites the CN stretch of the vibrational probes. The probes are excited preferentially along the direction of the pump pulse's electric field. The probability of a CN being excited is at its maximum when parallel to the pump's E-field, while the probability is zero when perpendicular. After a time delay, t, the probe pulse passes through the pumped spot in the sample. Because of the 0-to-1 transition excitation by the pump pulse, the probe pulse experiences increased transmission (positive signal) due to ground state bleaching and stimulated emission from the first excited state, 1. With a population in 1, a new absorption (negative signal) is created, the 1−2 transition, which is shifted to a lower frequency by the vibrational anharmonicity. A four-shot phase cycling of the pump pulse is used to extract the signal while removing pump scatters.[53]

Measurements of the probe transmitted intensity are made for the probe pulse parallel, $I_{\parallel}$, and perpendicular, $I_{\perp}$, to the pump pulse. The probe parallel to the pump will experience more excited CNs; therefore, there will be more transmission intensity than that of the probe perpendicular to it. At very short t, the difference between $I_{\parallel}$ and $I_{\perp}$ is maximum. As the probe molecules reorient, the initially excited CNs change direction and the difference between $I_{\parallel}$ and $I_{\perp}$ decreases. If the probe molecules could randomize their orientations, then the difference between $I_{\parallel}$ and $I_{\perp}$ would decay to zero. This is not the case for probes embedded in polymer samples, as discussed briefly above, because the probes are too large to undergo complete reorientation. They hit the walls of the FVEs and can only sample a limited range of angles determined by the length of the probe molecular ruler and the radius of the FVE. The extent of the decay allows the cone angle to be determined. The cone angle can be determined by measuring $I_{\parallel}$ and $I_{\perp}$.

The time dependence of $I_{\parallel}$ and $I_{\perp}$ signals is given by[54,55]

$$I_{\parallel} = P(t)(1 + 0.8C_2(t))$$
$$I_{\perp} = P(t)(1 - 0.4C_2(t)) \quad (1)$$

where $P(t)$ is the population relaxation (vibrational lifetime of the CN mode) and $C_2(t)$ is the second Legendre polynomial orientational time correlation function for the transition dipole, which contains the information on the orientational dynamics of the probe molecule. The population relaxation, $P(t)$, and the anisotropy, $r(t)$, can be obtained by combining the parallel and perpendicular signals

$$P(t) = \frac{1}{3}(I_{\parallel}(t) + 2I_{\perp}(t))$$
$$r(t) = \left(\frac{I_{\parallel}(t) - I_{\perp}(t)}{I_{\parallel}(t) + 2I_{\perp}(t)}\right) = 0.4C_2(t) \quad (2)$$

Experimental determination of $r(t)$ gives $C_2(t)$.

3. RESTRICTED ORIENTATION ANISOTROPY METHOD (ROAM)

A detailed description and explanation of ROAM have been published previously.[42,43] The tests and improvements in the technique presented here do not change the ROAM method. Here, we include an overview of the fundamental methodology, i.e., extraction of cone angles from the PSPP experiment and the maximum entropy method to extract RPDs. The improvements in the technique will be discussed in the following sections.

ROAM utilizes the PSPP experiment discussed above to measure $r(t)$, the time-dependent anisotropy decay, of the probe molecules embedded in the FVEs over a range of frequencies within the inhomogeneously broadened CN stretch absorption spectrum. The anisotropy would decay to zero in a low-viscosity liquid because the probe can sample all angles. In a glassy polymer, however, the anisotropy decays to a constant offset because the probes can sample only a limited range of angles defined by the sizes of FVEs. At different frequencies of the absorption spectrum, the anisotropy decays

https://doi.org/10.1021/acs.macromol.3c02093
Macromolecules XXXX, XXX, XXX−XXX

vary because subensembles of probes confined in FVEs of different sizes experience distinct frequencies. As the frequency changes from high frequency (blue) to low frequency (red), the sizes of the FVEs become smaller. Therefore, by measuring the $r(t)$ decays across the vibrational spectrum, information is obtained on the distribution of FVE sizes.

The experimentally measured anisotropy decays can be analyzed by the wobbling-in-a-cone (WIAC) theory.[44−46,56] WIAC has been used extensively in IR PSPP experiments to analyze orientational motions in a wide variety of systems.[57−60] In the context of polymers, the WIAC model is used to extract the cone half angles sampled by the probe molecules confined in FVEs. $C_2(t)$ for WIAC is given by the following expression[61]

$$C_2(t) = S_0^2(S_1^2 + (1 - S_1^2)\exp(-t/\tau_1))(S_2^2 + (1 - S_2^2)\exp(-t/\tau_2)) \quad (3)$$

where S_0, S_1, and S_2 are order parameters describing the ranges of reorientations, which can be expressed in terms of the cone angles

$$S_i = \frac{1}{2}\cos(\theta_i)(1 + \cos(\theta_i)) \quad (4)$$

S_0S_1 is converted to θ_{fast}, which describes the fast diffusive motion that occurs on a time scale <10 ps in the experiments presented below. θ_{fast} is the maximum angle that the probe molecules sampled in the immediately accessible space within FVEs, which, at the different frequencies, corresponds to the different sizes of the free volume elements. S_2 is associated with θ_{slow}, which describes angular sampling on a much longer time scale. The nature of θ_{slow} will be discussed in Section 4E. The conversion from the order parameters to θ_{fast} and θ_{slow} is given in eq 5

$$\theta_{fast} = \cos^{-1}\left(\frac{1}{2}(\sqrt{8S_0S_1 + 1} - 1)\right)$$

$$\theta_{slow} = \theta_{tot} - \theta_{fast} = \cos^{-1}\left(\frac{1}{2}(\sqrt{8S_0S_1S_2 + 1} - 1)\right) - \theta_{fast} \quad (5)$$

Determining the cone angles sampled by a vibrational probe in an FVE contains no assumptions. $C_2(t)$, the transition dipole second Legendre polynomial orientational time correlation function, is rigorous. It gives the angles sampled. The equations given in eqs 3 and 4 were developed in the context of the WIAC theory.[61] However, the WIAC theory is only necessary to understand how the time constant is related to the cone angle.[56]

Once the cone angles are obtained, the conversion from cone angles to FVE radii requires models for the FVE shape and how the probe molecules' maximum angular sampling is determined by contact with the FVE surface. For ROAM, the FVEs are modeled as cylinders with walls that limit the probe molecules' orientational motions. The radii of the cylindrical FVEs can be obtained with the molecular ruler length of the probe molecule. Based on the results of this paper, we will validate the assumption of cylindrical FVEs over a length scale somewhat longer than the longest probe molecule and provide an improved method for determining the length of the probe molecules. The cone angles are converted to radii by using the different lengths of the six probe molecules.

Using the frequency-dependent radii and the absorption spectrum, the radius probability distribution (RPD) can be obtained using the method presented previously.[43] The RPD is obtained using the principle of maximum entropy by combining the FVE radii measurement at each frequency with the population distribution of frequencies from the linear absorption spectrum. The expectation value of frequency-dependent FVE radii can be expressed using the following equation

$$\langle R(\omega)\rangle = \frac{1}{\rho(\omega)}\int_0^\infty \rho(\omega|R)\rho(R)R\,dR \quad (6)$$

where $\rho(\omega)$ is the area normalized linear absorption spectrum of the vibrational probe in the polymer sample. $\rho(\omega|R)$ is the conditional probability density function of probe molecules having frequency ω given it is in an FVE of radius R. $\rho(\omega)$ is the desired radius probability distribution function for the FVE. $\rho(\omega|R)$ is taken to be Gaussian with exponentially increasing width with respect to decreasing radius, which is consistent with simulation results for polystyrene oligomers.[43] The parameters for $\rho(\omega|R)$ are iterated to simultaneously reproduce both $\rho(\omega)$ and $\langle R(\omega)\rangle$, which greatly constrains the fit, yielding a robust determination of the RPD.

4. RESULTS

Since significant temperature fluctuation would affect the FVE size and size distribution, all PSPP experiments are conducted in a temperature-controlled laser room at 21.8 °C.

4.1. PhSeCN/PhSCN in Polystyrene. Previously, ROAM was used to study FVEs in polystyrene, with PhSeCN as the vibrational probe. In this section, we present PhSCN and PhSeCN data and compare the results. The linear absorption spectra of PhSeCN and PhSCN in polystyrene are given in Figure 1. Both spectra are fitted with Gaussian functions on the high-frequency side, and the fits are extended to the low-frequency side to obtain the center frequency, the full width at half-maximum (fwhm), and to show the tails of the absorptions to low frequency. The center frequency of PhSeCN is 2155.4 ± 0.1 cm^{-1} with a fwhm of 8.4 ± 0.1 cm^{-1}. Similarly, the center frequency of PhSCN is 2158.5 ± 0.1 cm^{-1} with a fwhm of 8.0 ± 0.1 cm^{-1}. Compared to PhSeCN, the linear

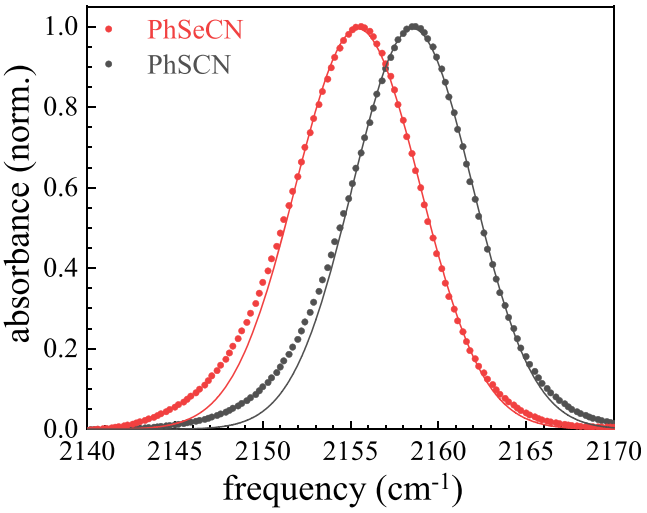

Figure 1. FTIR spectra of the CN stretch of PhSeCN (red) and PhSCN (black). The lines are Gaussian fits to the high-frequency sides of the spectra, which were then extended to the low frequencies to highlight the non-Gaussian distribution.

https://doi.org/10.1021/acs.macromol.3c02093
Macromolecules XXXX, XXX, XXX−XXX

absorption spectrum of PhSCN has a slightly blue-shifted center frequency with almost the same shape. The similarities in the spectra are consistent with the two molecules having very similar chemical structures. At high frequencies, both spectra are well-described by Gaussian functions.

The spectra deviate from the Gaussian fit on the low-frequency side. The Stark effect on the frequency of the CN stretch dominates the inhomogeneous widths and the line shapes.[62] The deviation from Gaussian line shapes is a manifestation of the non-Gaussian distribution of electric fields in the FVEs, which gives rise to non-Gaussian frequency dependence.

In the previous papers using ROAM to measure polymer FVE radii and RPDs, it was shown that PhSeCN exhibited frequency-dependent anisotropy decays in a variety of polymers.[16,42,43] This feature is central to determining the RPD. Figure 2A shows the anisotropy decays ($r(t)$, eq 2) of PhSCN in PS. The decays display a frequency dependence that is very similar to that of the decay of PhSeCN in PS. The anisotropy curves are fitted with biexponential functions and a constant offset. At the center frequency, the first decay time constant (t_1) for PhSCN is 2.5 ± 0.5 ps, and the second time constant (t_2) is 30 ± 10 ps. Both time constants are significantly faster than the PhSeCN time constants, which are 6.6 ± 0.5 ps (t_1) and 150 ± 10 ps (t_2). The set of PhSeCN decays is shown in the SI. The anisotropy decays of both probes at their respective center frequencies are shown in Figure 2B. The PhSCN decays faster to a smaller constant offset, showing that PhSCN molecules undergo orientational relaxation through a greater range of angles. With sulfur (S) in between the phenyl ring and the nitrile instead of selenium (Se), the overall size of the PhSCN molecule is smaller than that of PhSeCN. As will be discussed in detail below in the context of the calculations of the appropriate lengths for probe molecules, a smaller probe samples a larger cone angle in FVEs of the same size.

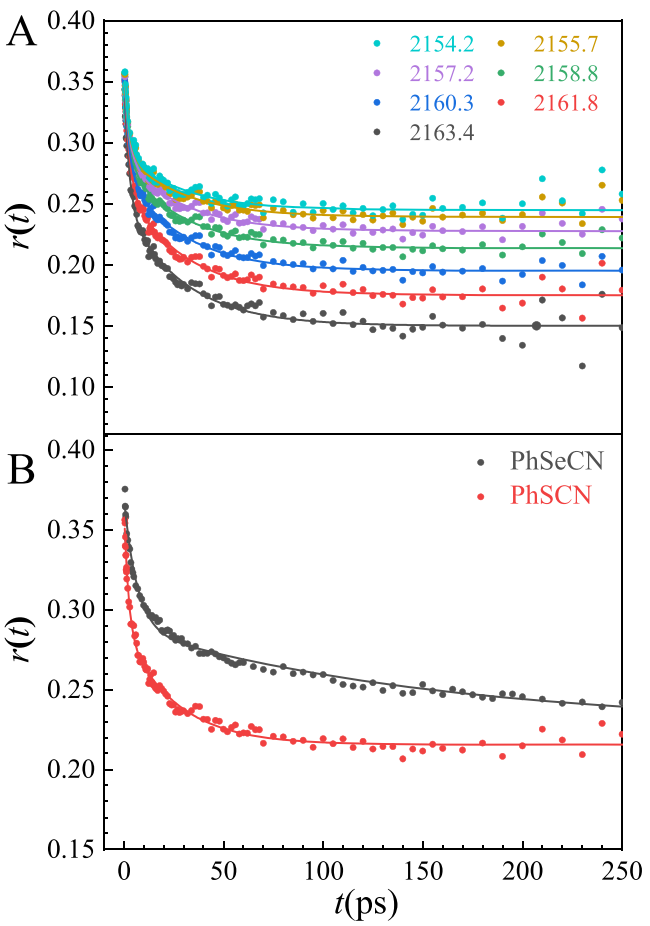

Figure 2. Anisotropy decay data for PhSCN and PhSeCN in polystyrene. (A) Frequency-dependent anisotropy decay data for PhSCN. (B) The anisotropy decays for PhSCN and PhSeCN at their respective center frequencies. The PhSCN anisotropy decays faster to a lower value of the long-time offset than PhSeCN. The solid lines are the fits to the experimental data using biexponential decays plus constant offsets.

4.2. *p*-Substituted Benzonitriles (*p*-XBZN) in Polystyrene. In addition to PhSeCN and PhSCN, benzonitrile derivatives with halogens (F, Cl, Br, and I) at the para-position were also studied. Their geometries are simpler to model than PhSeCN and PhSCN, and they do not have an internal rotation. By variation of the size of the atom at the para-position, the effect of length can be systematically studied while maintaining the same molecular shape. The linear absorption spectra of *p*-FBZN, *p*-ClBZN, *p*-BrBZN, and *p*-IBZN are displayed in Figure 3. The center frequencies and

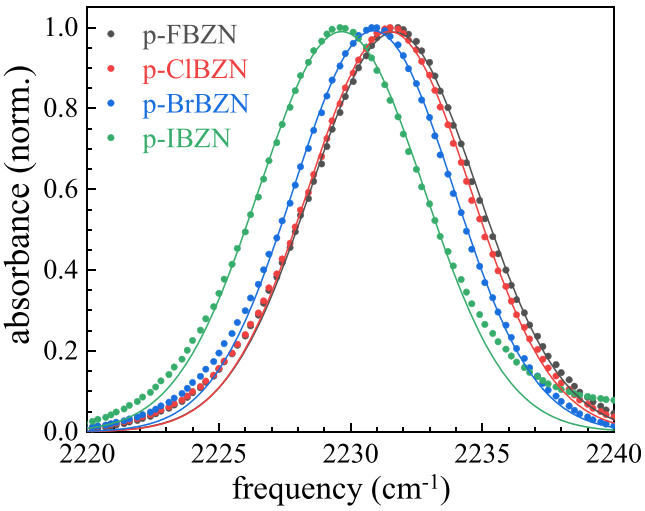

Figure 3. FTIR spectra of the CN stretch of *p*-FBZN (black), *p*-ClBZN (red), *p*-BrBZN (blue), and *p*-IBZN (green). The lines are Gaussian fits to the high-frequency sides of the spectra, which were then extended to the low frequencies to highlight the non-Gaussian distribution. The center frequency of the probe decreases with increasing mass of the para-substituents.

fwhm's are extracted by fitting the high-frequency sides of the spectra with a Gaussian function. The center frequencies of the p-XBZN probes decrease slightly with increasing mass of the para-substituents (~2 cm^{-1}, see Table S1). In addition, the center frequencies of the *p*-XBZN probes are blue-shifted by almost 80 cm^{-1} compared to those of PhSeCN and PhSCN.

A complication involved with collecting anisotropy decay of the *para*-substituted benzonitrile is that the pump−probe signal has a negative feature that is red-shifted relative to the peaks of the 0-to-1 transitions (Figure S5). The coupling between the CN stretch mode and phenyl ring modes causes this phenomenon. Following excitation by the pump pulse, the excited state population relaxes with the vibrational lifetime, and a low-frequency mode of the molecule is populated. The

https://doi.org/10.1021/acs.macromol.3c02093
Macromolecules XXXX, XXX, XXX−XXX

population of the low-frequency mode results in a combination band shift that grows with increasing delay time, t.[63] The growth of the combination band overlaps with the 0-to-1 transition signal, preventing accurate analysis of the pump−probe data. Because the 1-to-2 transition only arises from molecules in the excited states, probing this transition avoids the combination band problem while providing the same information as the 0-to-1 transition.[62] Therefore, the PSPP data for all four p-XBZN are collected using the 1-to-2 signals. The *p*-XBZN probes have much shorter excited state lifetimes than PhSeCN due to the increased coupling strength between nitriles and the ring modes caused by the absence of a heavy atom. *p*-FBZN, p-ClBZN, *p*-BrBZN, and *p*-IBZN have vibrational lifetimes of 11.7 ± 0.1, 21.5 ± 0.1, 11.4 ± 0.1, and 6.2 ± 0.1 ps, respectively (see Figure S6). Among these four probes, *p*-ClBZN has the longest vibrational lifetime. Note that even the *p*-ClBZN lifetime, 21.5 ps, is ∼20 times shorter than the lifetime of PhSeCN. The p-ClBZN anisotropy data at three frequencies are shown in Figure 4A as an example. The anisotropy data for the other *p*-XBZN probes behave similarly. As with PhSeCN and PhSCN, the *p*-ClBZN anisotropy decay is biexponential to an offset. At the center frequency, the first time constant is 1.0 ± 0.5 ps and the second time constant is 30 ± 5 ps. The anisotropy decay of, e.g., *p*-ClBZN in a low-viscosity liquid, DMF, is a perfect single exponential (see Figure S7). The different behaviors of *p*-ClBZN anisotropies in PS and DMF demonstrate that the biexponential decay in the polymer matrix arises from caging by the FVEs. In addition, the anisotropy shows a clear frequency dependence that is consistent with all previous observations. Compared to the anisotropy decays of PhSeCN and PhSCN, the red and blue wing decays of the *p*-XBZN anisotropies are not as different. A recent study shows that PhSeCN has a much larger Stark coupling constant than BZN and a much smaller non-Stark intermolecular coupling to its surroundings.[62] In the context of polymers, it has been previously established that probe molecules experience variable electric field strengths in FVEs of different sizes. For benzonitriles, the effect is that a given change in frequency corresponds to a smaller change in FVE size, i.e., a small change in the anisotropy decay. Because of the smaller Stark couplings, the combination band issue, and the short vibrational lifetimes, the determination of RPD using *p*-XBZN probes is not possible. Since RPD is required to determine the average radius, for comparing all six probes, each probe's FVE radius at the center frequency (the peak of the FTIR spectrum) will be used. Using the most probable frequency is a consistent method of comparison.

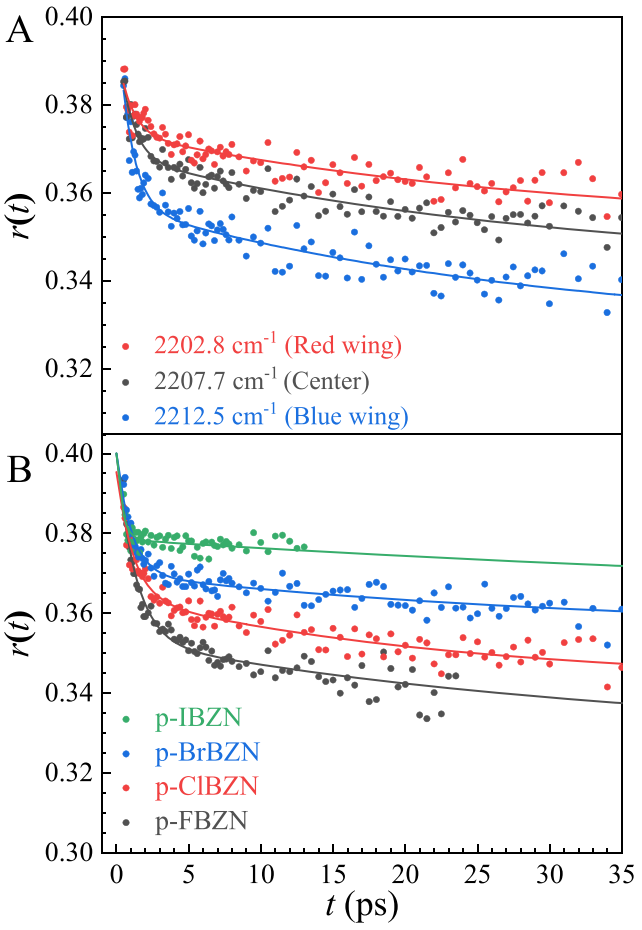

Figure 4. Anisotropy decay data for *p*-XBZN (X = F, Cl, Br, I) in polystyrene. (A) Frequency-dependent anisotropy of *p*-ClBZN. (B) The anisotropy decays for all four *p*-XBZN probes at their respective center frequencies. The probes decay to a larger offset (larger value at long time) with an increasing size of the para-substituent. The solid lines are fits to the experimental data using biexponential decay plus a constant offset.

To highlight the effect of probe length on the anisotropy decay, the anisotropies at their respective center frequencies of all four XBZN probes are plotted in Figure 4B. As the para-substituent becomes smaller, the anisotropy decays to a greater extent to a smaller offset value. *p*-FBZN decays the most (black curve). At the end of the plot, 35 ps, the value of the fit curve is 0.338. In contrast, *p*-IBZN decays the least (green curve) to 0.371. (Note that the lifetime of the CN stretch of *p*-IBZN is so short that the data are useful for only 13 ps.) The data show that a longer probe samples a smaller cone angle. PhSeCN and PhSCN display the same behavior.

5. DISCUSSION

5.1. *p*-XBZN Length and Contact Model. To obtain the FVE radii lengths based on the cone angles sampled by a probe molecule, we need to consider all orientational motions that lead to depolarization of the nitrile stretch. For *p*-XBZN probes, two scenarios need to be considered (Figure 5). Figure 5A represents the maximum angle sampled by the out-of-plane rotation of the probe. Figure 5B shows the in-plane rotation. The rotation around the CN axis is not considered because it does not cause depolarization. One important feature of the PSPP experiment is that the measured cone angle, θ_{fast}, is the maximum angle sampled by the probe molecule. Given the width of the phenyl ring, the out-of-plane motions give the largest angle (Figure 5A), i.e., the largest change in the direction of the CN bond vector (transition dipole). Therefore, we use A, the out-of-plane motion, to determine the lengths of *p*-XBZN and the atoms contacting the inner walls of the FVE. The contact atoms are halogen at the para-position and nitrogen (N) in the nitrile group. This physical picture is further supported by the fact that varying the size of the halogen changes the cone angle, demonstrating that one of the contacting moieties must be the halogen. To convert the cone angles into FVE radii, R, the following formula is used:

https://doi.org/10.1021/acs.macromol.3c02093
Macromolecules XXXX, XXX, XXX−XXX

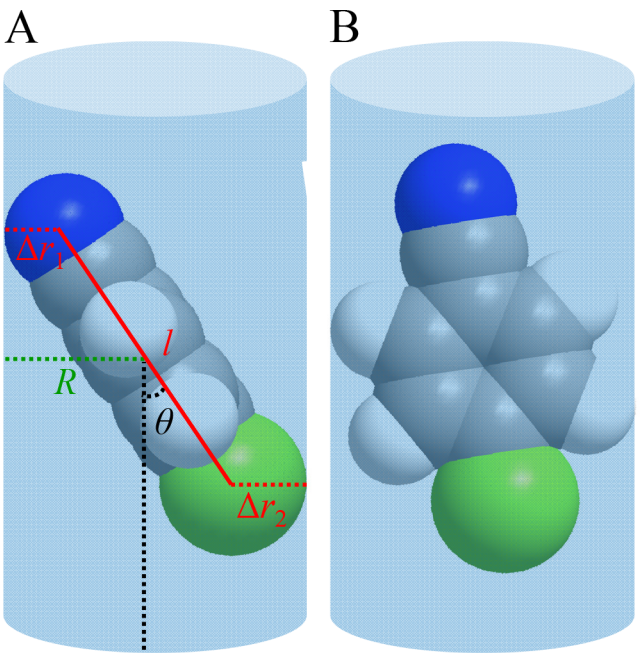

Figure 5. Two possible contact models of *p*-XBZN probes inside a cylinder. (A) The nitrogen and the halogen contact the FVE. This scenario is adopted to model *p*-XBZN probes because it produces the largest angle. (B) Two hydrogens contact the FVE.

$$R = \frac{1}{2}(l \sin(\theta) + \Delta r_1 + \Delta r_2) \tag{7}$$

where l is the length of the probe from the center of N to the center of the halogen and Δr_1 and Δr_2 are the van der Waals (vdW) radii of the two atoms contacting the FVE walls, which are N and the halogen in this case. The determination of the vdW radii is discussed in Section 5.3 below.

5.2. PhSeCN/PhSCN Revised Model. Similar to considering the *p*-XBZN probes, two scenarios for PhSeCN/PhSCN are shown in Figure 6. The rotations in the plane of the phenyl ring are not considered since the CN is nearly perpendicular to this plane; therefore, depolarization from in-plane rotation is negligible. For the first case, the two contacting moieties are the Se/S atom and the hydrogen atom at the *para*-position (*p*-H; Figure 6A). In the second case, the two contacting moieties are N and *para*-H/carbon (Figure 6B). Since the Se to *p*-H distance is shorter than the N to H distance, scenario (A) results in a larger maximum cone angle and is used for PhSeCN/PhSCN. In general, a shorter distance will yield a larger cone angle. The motion of the line along the shortest distance that changes the transition dipole direction determines the FVE radii. The conversion from cone angles to radii uses the same equation as the *p*-XBZN model (eq 7), except l is the distance from the center of S/Se to the center of *p*-H, and the vdW radii used are the radii of Se/S and H.

The complete parameters used for all six probes are listed in Table 1. The earlier model for PhSeCN assumed the probe molecule rotates around its center of mass and used the longest length from the center of mass as the rotating arm.[42] However, this model for PhSeCN does not accurately describe the moieties that contact the FVE surfaces. Given the same cone angle, the old model yielded somewhat larger FVE radii but did not change the shapes of the RPDs.[16]

5.3. Consistent FVE Radii Measurements from Six Probes. The cone angle, θ_{fast}, sampled by each type of probe molecule is plotted against the length of the probe (distance between the centers of the two contacting moieties) in Figure 7. It can be observed that all six vibrational probes follow the same trend with a linear relationship. Going from PhSCN to p-IBZN, the molecule becomes considerably longer and the measured θ_{fast} is smaller. This is consistent with the picture that in a cylindrical element with a fixed radius, a longer stick can rotate through a smaller angle before the cylinder wall restricts it.

So far, we have discussed the modeling schemes for the p-XBZN and PhSeCN/PhSCN probes. The only parameters left to convert the cone angles to FVE radii are the van der Waals (vdW) radii of the moieties that contact the walls of the FVE (see Figures 5 and 6).[42] Previously, the vdW radii used were based on the length recommended by Bondi from 1964,[64] which were determined from X-ray data and assumed to be isotropic. The updated considerations for the choices of vdW radii are presented here.

It has been known from thorough charge distribution analysis and statistical analysis that the vdW radii of atoms in bonded molecules are anisotropic and the transverse radii (R_t)

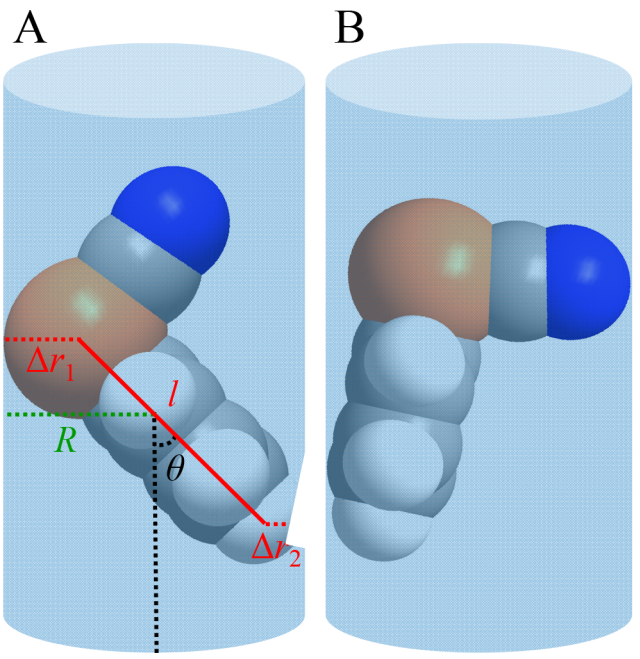

Figure 6. Two possible contact models of PhSeCN/PhSCN inside a cylinder. (A) The Se/S and para-hydrogen contact the FVE. This scenario is adopted for modeling PhSeCN/PhSCN since it produces the largest angle. (B) The nitrogen and the para-hydrogen contact the FVE.

Table 1. Model Parameters for Converting Fast Cone Angles to FVE Radii[a]

vibrational probes	l (Å)	Δr_1 (Å)	Δr_2 (Å)
PhSCN	5.67	2.03 (S)	1.0 (H)
PhSeCN	5.81	2.12 (Se)	1.0 (H)
p-FBZN	6.69	1.75 (F)	1.95 (N)
p-ClBZN	7.11	1.94 (Cl)	1.95 (N)
p-BrBZN	7.27	2.05 (Br)	1.95 (N)
p-IBZN	7.50	2.54 (I)	1.95 (N)

[a] l is the length of the molecules between the center of the two moieties that contact the FVE walls; Δr_1 and Δr_2 are the vdW radii of the atoms that collide with the FVE walls.

https://doi.org/10.1021/acs.macromol.3c02093
Macromolecules XXXX, XXX, XXX−XXX

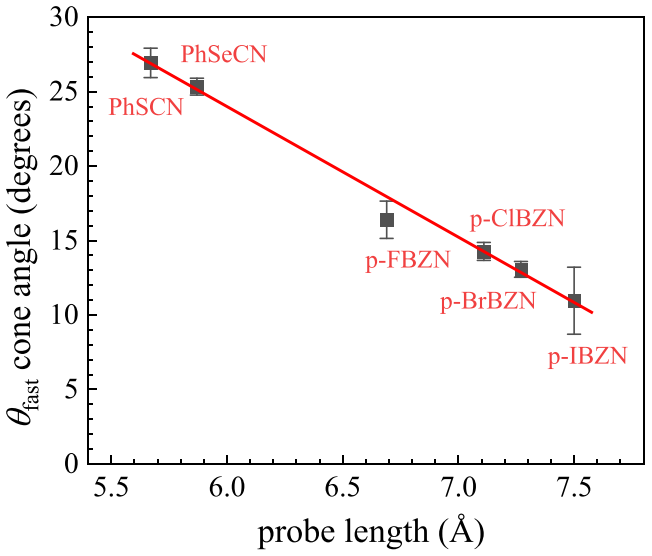

Figure 7. Cone angles θ_{fast} vs the probe molecular ruler length. A longer probe produces a smaller θ_{fast} cone angle. The length of the probe is the distance between the centers of two atoms that contact the FVE walls.

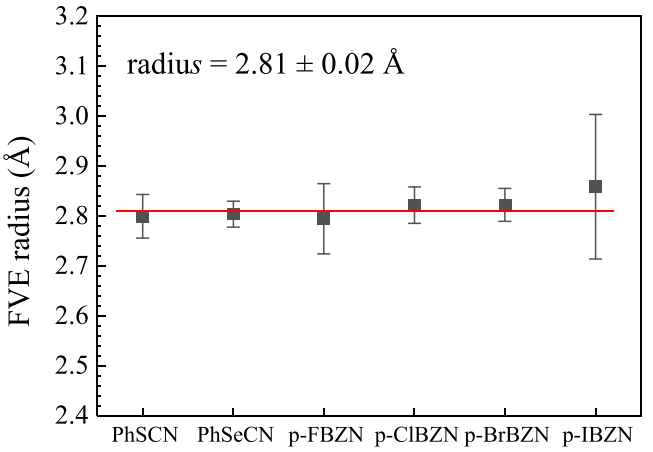

Figure 8. FVE radii from the cone angles for each probe at its FTIR absorption peak frequency. All six probes produce the same FVE radius within error with an average of 2.81 ± 0.02 Å. The red line is a guide for the eye.

are always larger than longitudinal radii (R_l).[65,66] The difference between R_t and R_l can be as large as 0.7 Å;[67] therefore, it is critical to include the effect of the anisotropy when considering the vdW radii of the atoms contacting the FVE surface. For *p*-XBZN probes, the N and the halogen at each end of the molecules contact the FVE walls in the transverse direction to their respective chemical bonds. In PhSeCN/PhSCN molecules, the transverse vdW radii should be used for hydrogen in the para-position for the same reason. However, because the Se and S atoms are bonded to two carbons with close to 90° angle between them, the average of R_t and R_l is appropriate. For isolated vibrational probe molecules occupying polymer FVEs, the environment around the probes is closer to the gas phase than densely packed molecular crystals because polymer FVEs are considered unoccupied space formed by imperfect packing.[68] For this reason, the vdW radii used for the updated model are from gas-phase measurements when available. For Cl, Br, and N atoms, the transverse vdW radii values determined by Batsanov in 1998 are used, which are measured on X_2 molecules using a series of noble gases.[69] Given that F, S, and Se data are not available from the same source, the semiempirical estimates from equilibrium vdW radii are used, which are the closest values to the noble gas measurements.[70] The same semi-empirical estimate is used for iodine because accurate experimental measurements of iodine are unavailable. The vdW radius of hydrogen varies dramatically from source to source.[64,71] In addition, hydrogen is a unique case, where the vdW radius would decrease when it is bonded to carbon.[67] The most appropriate data to use is the measurement of the H−H contact distance between two aromatic rings.[64] The vdW radius values used are given in Table 1.

Using the updated vdW radii, the θ_{fast} measured with the six probes can be converted to the FVE radii using eq 7. The results shown in Figure 8 are the polystyrene FVE radii. The average of the six points is 2.81 ± 0.02 Å.

This value is the radius at the peak of the absorption spectrum. The large error bar for the *p*-IBZN probe is caused by its short lifetime, which limits the range of data that can be collected.

The most important aspect of Figure 8 is that six different probes give the same FVE radius within experimental error. The probes have different lengths and different geometries. Four might be termed straight, while two are bent. Two have internal rotation (discussed below), while the other four do not. These results are a rigorous test and confirm the ROAM method. Although some aspects of the methodology have been improved, the basic principles underlying ROAM have not changed since the initial presentations.[42] It is important to state that determining the cone angles from the anisotropy measurements does not depend on assumptions. Modeling comes in when the cone angles are converted to radii. Here, we present more accurate methods of assigning the molecular ruler length for probes with different geometries.

The results presented in Figure 8 strongly support a fundamental assumption of the method: the ensemble average FVE shape is cylindrical on a length scale that is at least somewhat longer than the longest probe molecule studied. The FVEs cannot be spheres for the following reasons. If the length of the probe was smaller than the sphere radius, it would be able to sample all angles. If the length of the probe was larger than the sphere radius, it would essentially be unable to sample any angles. As stated above, the ensemble average at a given wavelength is associated with a particular cylindrical radius. However, the surface will not be smooth. As discussed below, there is evidence for surface roughness.

5.4. Internal Rotations. In PhSeCN, the nitrile group can rotate around the C(Ph)-Se bond if the rotation barrier is small enough. The internal rotation of CN can create anisotropy decay that is not due to the wobbling motion that samples the FVE size, as discussed above. Such internal rotation might complicate the ROAM measurements. One important question needs to be answered. Does internal rotation depolarization interfere with the method described above? In this section, it is demonstrated that, although internal rotation does happen for PhSeCN-like molecules, the amplitude of the internal rotation is not large enough to contribute to θ_{fast} that is used to determine the FVE size. To this end, PhSeCN and PhSCN are compared. As shown in Figure 8, these two probes yield the

https://doi.org/10.1021/acs.macromol.3c02093
Macromolecules XXXX, XXX, XXX−XXX

same size FVE and are the same as the other four probes that do not have an internal rotation.

PES calculations for PhSeCN and PhSCN were performed with DFT to determine the barriers for internal rotation (Figure S8). The maximum energies of the PES are the internal rotation barriers, which are 0.34 kcal/mol for PhSeCN and 0.07 kcal/mol for PhSCN. The two rotation barriers are very different but both are below RT at 298 K (0.59 kcal/mol). Therefore, the energy barriers are not large enough to prohibit internal rotation. In contrast, the geometries of the p-XBZN probes do not permit internal rotation. In Section 5.2, we have shown that the first exponential decay of *p*-ClBZN comes from the confinement effect of the FVEs because, in the absence of confinement, the decay is a single exponential (see Figure S7). Therefore, the first exponentials of PhSeCN and PhSCN have contributions from both the confinement effect by the FVEs and internal rotation. If the internal rotation determines the fast cone angle, one would see significant differences among radii measured by PhSeCN, PhSCN, and radii measured by the *p*-XBZN probes as they have drastically different internal rotation characteristics. Therefore, the data demonstrate that θ_{fast} is determined by the WIAC sampling instead of internal rotation. Internal rotation does occur for PhSeCN and PhSCN molecules, but the range of angle sampled by the internal rotation is smaller than the cone angle from the wobbling motion.

Internal rotation does play a role in the rate of angular sampling. When comparing the PhSeCN and PhSCN time constants that give rise to θ_{fast} and the slower long-time decay constants, we see that both time constants for PhSCN are significantly faster than those for PhSeCN. This phenomenon can be attributed to PhSCN having a smaller internal rotation barrier, making it much more mobile inside a highly confined FVE, and enabling it to sample the same-sized FVE faster, as seen qualitatively from Figure 6. In part B, the probe is against the FVE surface but in a configuration that does not sample the largest angle. To get to the configuration in A without internal rotation requires thermal angular fluctuations that move the probe from being pinned against the wall, as in B. Rotation of the −SCN moiety releases the probe from its B configuration without the entire molecule rotating. This will speed up the search of all angular configurations, allowing for the A configuration to be found more rapidly. PhSCN has a lower barrier than PhSeCN. Therefore, the internal rotation will sample a range of angles faster, resulting in a faster decay of the fast anisotropy to the order parameter that yields θ_{fast}. The important point is that it is not the rate of angular sampling but the maximum cone angle sampled that is used to determine the FVE radius.

5.5. Slow Cone, θ_{slow}. The anisotropy data for all six vibrational probes exhibit biexponential anisotropy decays, independent of whether the probe has internal rotation. The fast decay (<10 ps) is attributed to the angular sampling of the immediately accessible space (FVE). Different probes generate different θ_{fast} values (see Figure 7) on the short time scale because of the different molecular ruler lengths. Similarly, the slow decays of PhSCN, PhSeCN, and *p*-ClBZN also sample different additional angular ranges, θ_{slow}, which are 9.1 ± 1.1, 8.0 ± 0.6, and 4.0 ± 0.7°, respectively. (Of the halogenated probes, only p-ClBZN has a long enough lifetime to get reasonable longer time data.) However, the percent changes in the angular ranges sampled are the same within error, which are 34 ± 4, 32 ± 2, and 28 ± 5% for PhSCN, PhSeCN, and *p*-ClBZN, respectively.

In the initial development of ROAM, which used only PhSeCN as the vibration probe, the slow anisotropy decay was ascribed to changes in accessible angular space caused by shape and center position fluctuations that did not change the ensemble-averaged size of the FVE. The slow decay time constant, ∼150 ps, was attributed to the time required for the FVE shape fluctuations to occur by, e.g., side group and short-chain segment movements.[42,43] However, the slow decay time constant for PhSCN reported in this work is ∼30 ps, much smaller than that for PhSeCN (∼150 ps). Therefore, the time constant cannot be associated with the shape and center dynamics time, which would be independent of the probe. The comparison between PhSCN and PhSeCN shows that the slow decay time constant is not a measurement of polymer dynamics per se but instead involves the angular sampling rate of the specific probe. Nevertheless, the anisotropy data (Figure 2) unambiguously shows the existence of additional angular sampling at a rate ≥10 times slower than the fast angular sampling that determines the FVE radii.

Based on the existing evidence, we propose a new model for slow anisotropy decay. As in the original model, the walls of the FVEs should not be viewed as static. Quasielastic neutron scattering has demonstrated that the phenyl rings of atactic polystyrene below T_g can undergo orientational motions coupled to the main chain movements on multipicosecond time scales.[72] Similar dynamics are also observed for poly(methyl methacrylate)[73] and other polymers. These motions will cause fluctuations of the FVE surface topography around the average configuration. At short times, the probes sample the ensemble average configuration that is immediately accessible, which reports θ_{fast}, yielding the FVE radius. On the longer time scale, the fluctuations of the FVE surfaces open an additional angular space, but this space is transitory. For example, a thermal fluctuation causes a side group to move out of its lowest energy configuration into a new configuration that opens up angular space not sampled on the short time scale of θ_{fast}. After a short time, the new configuration returns to its original configuration. In the initial sampling that gives θ_{fast}, the probe is unlikely to find these transitory spaces. However, as the sampling continues, and with enough time, the topography fluctuations are encountered, which causes the probe to sample a larger angular space. There are also topographical fluctuations that transiently reduce the angular space. But these blocked spaces have already been sampled, so they do not cancel out newly opened spaces. For the short-time anisotropy decays that determined θ_{fast}, PhSCN had fast orientational relaxation because of the facile internal rotation of the SCN moiety. The faster sampling by PhSCN will occur on a long time scale, so it finds the topographical fluctuations more rapidly.

Consider walking quickly around a room, rolling a measuring wheel along the walls, as a rough analogy. There are closet doors, but the doors are closed, except for occasional brief openings. In the first circumnavigation of the room, the measuring wheel will measure its perimeter, as it is unlikely to encounter an open door. However, if many trips around the room are made, then some open doors will be encountered. The measuring wheel will trace out the walls inside the closets, adding to the measured perimeter.

Different probe lengths give rise to different fast decay times and θ_{fast} values but yield the same radius. Different probe

https://doi.org/10.1021/acs.macromol.3c02093
Macromolecules XXXX, XXX, XXX−XXX

lengths give rise to different slow decay times, but the same percent change in the angular range sampled within experimental error. The measurements are independent of which probe is used. However, as discussed in the next section, some probes are more useful than others.

5.6. Selecting a Probe for ROAM. In this work, we employed six different vibrational probes of varying sizes and geometries for ROAM measurements. The six probes yielded the same FVE radius within experimental error. The investigation of the six probes resulted in a more accurate model of probe geometry and molecular ruler length, although the basic ROAM method is unchanged. The original experiments used PhSeCN as the probe,[16,42,43] which is still the best choice for practical applications in various polymers because of two important features: lifetime and solvent coupling. In the PSPP experiment, the vibrational excited state lifetime needs to be longer than the orientational relaxation of the probe to achieve good data quality across the entire time window. This is especially a problem for *p*-FBZN, *p*-BrBZN, and *p*-IBZN, which have insufficiently long lifetimes to measure the slow cone accurately. *p*-ClBZN has a longer lifetime, but it is not long enough to accurately determine the second slow decay component. In contrast, PhSeCN has a lifetime significantly longer than that of the other probes (~400 ps), which ensures high-quality data collection beyond 600 ps. PhSCN also has a sufficiently long lifetime but shorter than PhSeCN. The long lifetime of these probes arises because the heavy atom effectively decouples the CN stretch from the high density of internal vibrational modes of the phenyl ring.[50,74]

The free volume element RPD is determined from a combination of the probe frequency distribution, i.e., the FTIR spectrum, and the PSPP measurement at each frequency. Therefore, to generate an accurate RPD, the different FVE sizes must be correlated to the probe frequency and broadly distributed across the CN absorption spectrum. This strong size-frequency correlation occurs when there is a large CN vibrational Stark coupling constant and a relatively weak frequency coupling to other intermolecular interactions. Experimental studies have measured the PhSeCN Stark coupling constant and the non-Stark coupling of the medium to the frequency.[42,62] Prior studies have shown that the electric field experienced by a probe in an FVE is directly related to the FVE size. The electric field becomes larger as the size decreases, and the vibrational Stark effect shifts the vibrational frequency to a lower frequency. Benzonitrile probes have much smaller Stark coupling constants and a larger non-Stark coupling of the frequency to the environment compared to PhSeCN.[62] The result is that the benzonitrile probes measure very similar FVE radii across the entire CN FTIR spectrum. Therefore, PhSeCN is an excellent vibrational probe for ROAM studies because of its long vibrational lifetime and strong Stark coupling. In addition, it is commercially available at a reasonable cost. Although other modes, such as carbonyls,[75] have strong Stark coupling, it is difficult to find small molecules with a mode with both strong Stark coupling and a long lifetime.

5.7. Polystyrene Radius Probability Distribution. With the updated model for PhSeCN, the FVE RPD in polystyrene has been recomputed using the new molecular ruler parametrization. The RPD is shown in Figure 9. The highly non-Gaussian distribution has the peak of the distribution at 2.7 Å and an average radius of 2.94 Å. For comparison, two separate

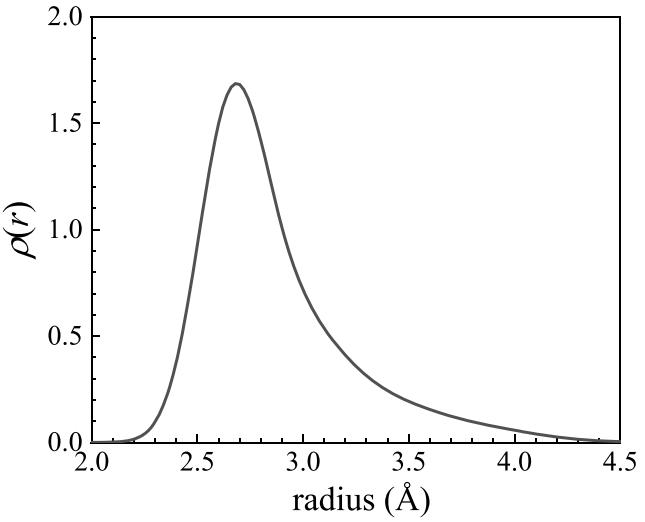

Figure 9. Radius probability distribution of polystyrene was measured with PhSeCN. The average radius is 2.94 Å, with the peak of the distribution at 2.69 Å.

PALS measurements of amorphous polystyrene resulted in similar annihilation lifetimes of 2.04[23] and 2.06 ns,[36] which can be converted[34,35] to average FVE radii of 2.88 and 2.90 Å, respectively. The average FVE radius of polystyrene from the ROAM measurements is remarkably close to the PALS result. Additionally, atomistic MD simulations of neat polystyrene have been conducted previously.[76] The simulation study produced a quantitative agreement with the PALS measurements and the ROAM measurements reported here on polystyrene FVEs. Furthermore, it showed that the shapes of the FVEs were far from spherical, which is a basic component of PALS analysis.

As discussed above in connection with Figure 8, the value determined by the six probes, 2.81 ± 0.02, was obtained using measurements of the peaks of their FTIR spectra. This value is different from the average value because the RPD is non-Gaussian. The average radius of the RPD reported here is smaller than the previously published one[43] because of the improved molecular ruler. The shapes of the RPDs are very similar to a long tail extending to large radii. Although the model for converting the fast cone angles to FVE radii has been updated here, the comparisons made in a previous publication[16] depended only on RPD shapes for several polymers. The change in the molecular ruler length does not affect comparisons among θ_{fast}, which are the direct experimental observables independent of the choice of the ruler length.

6. CONCLUDING REMARKS

In this paper, we have presented a rigorous test of ROAM by comparing the results of six different probe molecules in the same polymer, polystyrene. We prove the basic concept that underlies ROAM by using six different probe molecules with different lengths, geometries, and extents of internal rotation. The six probes sample different angular ranges on different time scales but result in the same FVE radius, within a small experimental error, when the differences in the molecular ruler length are accounted for (Figure 8). These results confirm the accuracy and efficacy of ROAM.

An interesting question is whether the solvent-casting process causes the polymer chains to organize around the

https://doi.org/10.1021/acs.macromol.3c02093
Macromolecules XXXX, XXX, XXX−XXX

probes, resulting in the probes generating the sizes of the FVEs that they measure. Three pieces of information presented above show that this is not the case. Because these three items are spread throughout this work, it is worth recapitulating them here. First, the six probes are of different sizes and shapes. If the measured FVE size is determined by the specific dimensions of the vibrational probe used for the measurement, then the six distinct probes investigated in this study would result in different FVE sizes. As shown in Figure 8, analysis of the data for the six probes, based on their sizes and shapes, gives the same FVE size within a very small error. Second, in the discussion of the sample preparation, it was noted that during the drying process in a vacuum oven used to remove the solvent at temperatures kept below T_g, ∼50% of the probe molecules diffused out of the sample. As the samples were thick, ∼250 μm, the probes moved long distances from the locations they had at the end of the solvent casting process. Therefore, the probes did not occupy the FVEs created during sample preparation. Third, as discussed in connection with Figure 9, the average FVE size measured by ROAM is within a few hundredths of an Angstrom of the size determined by two independent PALS measurements. The PALS measurements are made on samples that do not have ROAM probe molecules, eliminating the possibility that the probes produced the size of the FVEs that were measured.

If bigger and bigger probes are put into the polymer until the sizes of the probes are too large to fit into the pre-existing FVEs, then one would observe less and less anisotropy decay until the anisotropy becomes almost flat. Only a small degree of anisotropy decay would occur because the vibrational probes are severely restricted in the polymer matrix, rather than in FVEs, and cannot undergo significant orientational relaxation.

We advanced the methodology given in the initial presentation of ROAM by treating several issues that had not been examined previously. An important new aspect of this work is the significant improvement in determining the molecular ruler length of probes having different geometries, including the vdW radii of the contacting moieties. These advances did not change the ROAM technique but made it significantly more accurate. The accuracy of the new molecular ruler length is confirmed by obtaining the same FVE radius with six probes. Another important component of this work was demonstrating that internal rotation around the moiety containing the CN group, on which the IR measurements are made, did not change the FVE size determination. Internal rotation can speed up angular sampling, which changes the time dependence of the observed anisotropy decays. However, the time dependences of the decays are not used to obtain the FVE radius. The range of angles sampled by the probe molecules was analyzed to obtain the FVE radius. The radii obtained by ROAM analysis were the same for probes with and without internal rotation.

Another important outcome of this work is that we demonstrated the ensemble-averaged FVE shape is a cylinder on a length scale somewhat longer than that of the longest vibrational probe. The appropriateness of the cylindrical model is confirmed by the fact that probes with different lengths yield the same FVE radius. This finding could inform the FVE shape modeling employed in other techniques such as PALS.

Finally, two other aspects of ROAM are worth recapitulating. The method has no assumptions through the steps of determining the cone angles. Determining the cone angles from PSPP measurements of the anisotropy is widely used to analyze fluorescence depolarization measurements and NMR experiments. Furthermore, since ROAM does not require any assumptions about the chemical environment surrounding the probes, it is a valuable method for directly comparing different polymer systems.

■ ASSOCIATED CONTENT

Supporting Information

The Supporting Information is available free of charge at https://pubs.acs.org/doi/10.1021/acs.macromol.3c02093.

NMR characterization for residual solvents; Gaussian fit parameters for linear absorption spectra; orientational dynamics in polystyrene; *p*-XBZN PSPP signals and lifetimes; single-exponential anisotropy decay of *p*-ClBZN in DMF; internal rotation barrier calculation (PDF)

■ AUTHOR INFORMATION

Corresponding Author

Michael D. Fayer − *Department of Chemistry, Stanford University, Stanford, California 94305, United States;* orcid.org/0000-0002-0021-1815; Phone: 650 723-4446; Email: fayer@stanford.edu

Authors

Junkun Pan − *Department of Chemistry, Stanford University, Stanford, California 94305, United States;* orcid.org/0000-0001-6128-1844

Aaron P. Charnay − *Department of Chemistry, Stanford University, Stanford, California 94305, United States;* orcid.org/0000-0003-1797-9465

Sebastian M. Fica-Contreras − *Department of Chemistry, Stanford University, Stanford, California 94305, United States;* orcid.org/0000-0003-4177-8436

Complete contact information is available at: https://pubs.acs.org/10.1021/acs.macromol.3c02093

Notes

The authors declare no competing financial interest.

■ ACKNOWLEDGMENTS

The authors thank Professor Minhaeng Cho, Department of Chemistry and Center for Multidimensional Spectroscopy, Korea University, and his research group for valuable discussions.

■ REFERENCES

(1) Baekeland, L. H.Method of Making Insoluble Products of Phenol and Formaldehyde. US942699A1907.

(2) Nambiar, S.; Yeow, J. T. Conductive polymer-based sensors for biomedical applications. *Biosens. Bioelectron.* **2011**, *26*, 1825−1832.

(3) Jancar, J.; Douglas, J. F.; Starr, F. W.; Kumar, S. K.; Cassagnau, P.; Lesser, A. J.; Sternstein, S. S.; Buehler, M. J. Current issues in research on structure−property relationships in polymer nanocomposites. *Polymer* **2010**, *51*, 3321−3343.

(4) History of the American Chemical Society Division of Polymeric Materials: Science and Engineering. In *Applied Polymer Science: 21st Century*; Craver, C. C., Ed.; Elsevier, 2000; pp 3−20.

(5) Huan, T. D.; Boggs, S.; Teyssedre, G.; Laurent, C.; Cakmak, M.; Kumar, S.; Ramprasad, R. Advanced polymeric dielectrics for high energy density applications. *Prog. Mater. Sci.* **2016**, *83*, 236−269.

(6) White, R. P.; Lipson, J. E. G. Free Volume in the Melt and How It Correlates with Experimental Glass Transition Temperatures: Results for a Large Set of Polymers. *ACS Macro. Lett.* **2015**, *4*, 588−592.
(7) Drioli, E.; Giorno, L. Encyclopedia of Membranes. 2016.
(8) Rutherford, S. W. Mechanism of Sorption and Diffusion in a High Free-Volume Polymer. *Ind. Eng. Chem. Res.* **2001**, *40*, 1370−1376.
(9) Arya, R. K.; Thapliyal, D.; Sharma, J.; Verros, G. D. Glassy Polymers—Diffusion, Sorption, Ageing and Applications. *Coatings* **2021**, *11*, No. 1049, DOI: 10.3390/coatings11091049.
(10) Alentiev, A. Y.; Yampolskii, Y. P. Free volume model and tradeoff relations of gas permeability and selectivity in glassy polymers. *J. Membr. Sci.* **2000**, *165*, 201−216.
(11) Yave, W.; Car, A.; Peinemann, K.-V.; Shaikh, M. Q.; Rätzke, K.; Faupel, F. Gas permeability and free volume in poly(amide-b-ethylene oxide)/polyethylene glycol blend membranes. *J. Membr. Sci.* **2009**, *339*, 177−183.
(12) Low, Z. X.; Budd, P. M.; Mckeown, N. B.; Patterson, D. A. Gas Permeation Properties, Physical Aging, and Its Mitigation in High Free Volume Glassy Polymers. *Chem. Rev.* **2018**, *118*, 5871−5911.
(13) Wilks, B. R.; Chung, W. J.; Ludovice, P. J.; Rezac, M. R.; Meakin, P.; Hill, A. J. Impact of average free-volume element size on transport in stereoisomers of polynorbornene. I. Properties at 35 °C. *J. Polym. Sci., Part B: Polym. Phys.* **2003**, *41*, 2185−2199.
(14) Yang, L.; Yang, L.; Ma, K.; Wang, Y.; Song, T.; Gong, L.; Sun, J.; Zhao, L.; Yang, Z.; Xu, J.; Wang, Q.; Guogang, Li.; Zhou, W. Free volume dependence of dielectric behaviour in sandwich-structured high dielectric performances of poly(vinylidene fluoride) composite films. *Nanoscale* **2021**, *13*, 300−310, DOI: 10.1039/D0NR06070D.
(15) Qin, H.; Feng, Y.; Liu, K.; Mi, J.; Zhang, L.; Tian, M. From Molecular-Scale Cavities to Nanoscale Dielectric Breakdown in Polydimethylsiloxane Induced by Local Electric Field. *Macromolecules* **2022**, *55*, 1690−1699.
(16) Fica-Contreras, S. M.; Li, Z.; Alamri, A.; Charnay, A. P.; Pan, J.; Wu, C.; Lockwood, J. R.; Yassin, O.; Shukla, S.; Sotzing, G.; Cao, Y.; Fayer, M. D. Synthetically tunable polymers, free volume element size distributions, and dielectric breakdown field strengths. *Mater. Today* **2023**, *67*, 57−67, DOI: 10.1016/j.mattod.2023.05.010.
(17) Artbauer, J. Electric strength of polymers. *J. Phys. D: Appl. Phys.* **1996**, *29*, 446−456.
(18) Zhang, J.; Chen, H.; Li, Y.; Suzuki, R.; Ohdaira, T.; Jean, Y. C. Free-volume distribution and glass transition of nano-scale polymeric films. *Radiat. Phys. Chem.* **2007**, *76*, 172−179.
(19) Rowe, B. W.; Pas, S. J.; Hill, A. J.; Suzuki, R.; Freeman, B. D.; Paul, D. R. A variable energy positron annihilation lifetime spectroscopy study of physical aging in thin glassy polymer films. *Polymer* **2009**, *50*, 6149−6156.
(20) Wang, X. Y.; Willmore, F. T.; Raharjo, R. D.; Wang, X.; Freeman, B. D.; Hill, A. J.; Sanchez, I. C. Molecular simulations of physical aging in polymer membrane materials. *J. Phys. Chem. B* **2006**, *110*, 16685−16693.
(21) Utpalla, P.; Sharma, S. K.; Deshpande, S. K.; Bahadur, J.; Sen, D.; Sahu, M.; Pujari, P. K. Role of free volumes and segmental dynamics on ion conductivity of PEO/LiTFSI solid polymer electrolytes filled with SiO(2) nanoparticles: a positron annihilation and broadband dielectric spectroscopy study. *Phys. Chem. Chem. Phys.* **2021**, *23*, 8585−8597.
(22) Utpalla, P.; Sharma, S. K.; Prakash, J.; Bahadur, J.; Sahu, M.; Pujari, P. K. Free volume structure at interphase region of poly (ethylene oxide)-Al2O3 nanorods composites based solid polymer electrolyte and its direct correlation with Li ion conductivity. *Solid State Ionics* **2022**, *375*, No. 115840, DOI: 10.1016/j.ssi.2021.115840.
(23) Liu, J.; Deng, Q.; Jean, Y. C. Free-volume distributions of polystyrene probed by positron annihilation: comparison with free-volume theories. *Macromolecules* **1993**, *26*, 7149−7155.
(24) Golemme, G.; Nagy, J. B.; Fonseca, A.; Algieri, C.; Yampolskii, Y. 129Xe-NMR study of free volume in amorphous perfluorinated polymers: comparsion with other methods. *Polymer* **2003**, *44*, 5039−5045.
(25) Nagasaka, B.; Eguchi, T.; Nakayama, H.; Nakamura, N.; Ito, Y. Positron annihilation and 129Xe NMR studies of free volume in polymers. *Radiat. Phys. Chem.* **2000**, *58*, 581−585.
(26) Simpson, J. H.; Wen; Jones, A. A.; Inglefield, P. T.; Bendler, J. T. Diffusion Coefficients of Xenon in Polystyrene Determined by Xenon-129 NMR Spectroscopy. *Macromolecules* **1996**, *29*, 2138−2142.
(27) Yampolskii, Y.; Belov, N. Investigation of Polymers by Inverse Gas Chromatography. *Macromolecules* **2015**, *48*, 6751−6767.
(28) Gregory, R. B. Free-volume and pore size distributions determined by numerical Laplace inversion of positron annihilation lifetime data. *J. Appl. Phys.* **1991**, *70*, 4665−4670.
(29) Shantarovich, V. P.; Utracki, L. A.; Jamieson, A. M. Positron annihilation and free volume studies in polymer glasses. *J. Polym. Sci., Part B: Polym. Phys.* **2008**, *46*, 2485−2503.
(30) Shpotyuk, O.; Ingram, A.; Shpotyuk, Y. Free-volume characterization of nanostructurized substances by positron annihilation lifetime spectroscopy. *Nucl. Instrum. Methods Phys. Res. B* **2018**, *416*, 102−109.
(31) Yampolskii, Y. P. Methods for investigation of the free volume in polymers. *Russ. Chem. Rev.* **2007**, *76*, 59−78.
(32) Hofmann, D.; Heuchel, M.; Yampolskii, Y.; Khotimskii, V.; Shantarovich, V. Free Volume Distributions in Ultrahigh and Lower Free Volume Polymers: Comparison between Molecular Modeling and Positron Lifetime Studies. *Macromolecules* **2002**, *35*, 2129−2140.
(33) Consolati, G.; Nichetti, D.; Quasso, F. Probing the Free Volume in Polymers by Means of Positron Annihilation Lifetime Spectroscopy. *Polymers* **2023**, *15*, No. 3128, DOI: 10.3390/polym15143128.
(34) Tao, S. J. Positronium Annihilation in Molecular Substances. *J. Chem. Phys.* **1972**, *56*, 5499−5510.
(35) Eldrup, M.; Lightbody, D.; Sherwood, J. N. The temperature dependence of positron lifetimes in solid pivalic acid. *Chem. Phys.* **1981**, *63*, 51−58.
(36) Olson, B. G.; Prodpran, T.; Jamieson, A. M.; Nazarenko, S. Positron annihilation in syndiotactic polystyrene containing α and β crystalline forms. *Polymer* **2002**, *43*, 6775−6784.
(37) Goworek, T.; Ciesielski, K.; Jasińska, B.; Wawryszczuk, J. Temperature variations of average o-Ps lifetime in porous media. *Radiat. Phys. Chem.* **2000**, *58*, 719−722.
(38) Jean, Y. C.; Shi, H. Positronium lifetime in an ellipsoidal free-volume hole of polymers. *J. Non-Cryst. Solids* **1994**, *172*−*174*, 806−814.
(39) Nakanishi, H.; Jean, Y. C. *Positrons and Positronium in Liquids*, Chapter 5; Elsevier, 1988.
(40) Byakov, V. M.; Stepanov, S. V. Microscopic surface tension of liquids with curved free boundary studied by positron annihilation. *Radiat. Phys. Chem.* **2000**, *58*, 687−692.
(41) Li, S.; Sun, J.; Li, Z.; Peng, H.; Gidley, D.; Ryan, E. T.; Yan. Evaluation of Pore Structure in Pure Silica Zeolite MFI Low-k Thin Films Using Positronium Annihilation Lifetime Spectroscopy. *J. Phys. Chem. B* **2004**, *108*, 11689−11692.
(42) Hoffman, D. J.; Fica-Contreras, S. M.; Fayer, M. D. Amorphous polymer dynamics and free volume element size distributions from ultrafast IR spectroscopy. *Proc. Natl. Acad. Sci. U.S.A.* **2020**, *117*, 13949−13958.
(43) Fica-Contreras, S. M.; Hoffman, D. J.; Pan, J.; Liang, C.; Fayer, M. D. Free Volume Element Sizes and Dynamics in Polystyrene and Poly(methyl methacrylate) Measured with Ultrafast Infrared Spectroscopy. *J. Am. Chem. Soc.* **2021**, *143*, 3583−3594.
(44) Wang, C. C.; Pecora, R. Time-correlation functions for restricted rotational diffusion. *J. Chem. Phys.* **1980**, *72*, 5333−5340.
(45) Lipari, G.; Szabo, A. Effect of librational motion on fluorescence depolarization and nuclear magnetic resonance relaxation in macromolecules and membranes. *Biophys. J.* **1980**, *30*, 489−506.

https://doi.org/10.1021/acs.macromol.3c02093
Macromolecules XXXX, XXX, XXX−XXX

(46) Lipari, G.; Szabo, A. Model-free approach to the interpretation of nuclear magnetic resonance relaxation in macromolecules. 1. Theory and range of validity. *J. Am. Chem. Soc.* **1982**, *104*, 4546−4559.
(47) Araiso, T.; Koyama, T. A picosecond fluorescence study of the cone angle of the wobbling motion of rod-like fluorophore in lipid bilayers. *Chem. Phys. Lipids* **1989**, *50*, 105−108.
(48) Chang, S. L.; Tjandra, N. Analysis of NMR relaxation data of biomolecules with slow domain motions using wobble-in-a-cone approximation. *J. Am. Chem. Soc.* **2001**, *123*, 11484−11485.
(49) Pastor, R. W.; Venable, R. M.; Feller, S. E. Lipid bilayers, NMR relaxation, and computer simulations. *Acc. Chem. Res.* **2002**, *35*, 438−446.
(50) Fica-Contreras, S. M.; Daniels, R.; Yassin, O.; Hoffman, D. J.; Pan, J.; Sotzing, G.; Fayer, M. D. Long Vibrational Lifetime R-Selenocyanate Probes for Ultrafast Infrared Spectroscopy: Properties and Synthesis. *J. Phys. Chem. B* **2021**, *125*, 8907−8918.
(51) Frisch, M.; Trucks, G.; Schlegel, H. B.; Scuseria, G.; Robb, M.; Cheeseman, J.; Scalmani, G.; Barone, V.; Petersson, G.; Nakatsuji, H. *Gaussian 16*; Gaussian, Inc.: Wallingford, CT, 2016.
(52) Shim, S. H.; Zanni, M. T. How to turn your pump-probe instrument into a multidimensional spectrometer: 2D IR and Vis spectroscopies via pulse shaping. *Phys. Chem. Chem. Phys.* **2009**, *11*, 748−761.
(53) Yan, C.; Nishida, J.; Yuan, R.; Fayer, M. D. Water of Hydration Dynamics in Minerals Gypsum and Bassanite: Ultrafast 2D IR Spectroscopy of Rocks. *J. Am. Chem. Soc.* **2016**, *138*, 9694−9703.
(54) Tokmakoff, A. Orientational correlation functions and polarization selectivity for nonlinear spectroscopy of isotropic media. I. Third order. *J. Chem. Phys.* **1996**, *105*, 1−12.
(55) Tan, H.-S.; Piletic, I. R.; Fayer, M. D. Polarization selective spectroscopy experiments: methodology and pitfalls. *J. Opt. Soc. Am. B* **2005**, *22*, 2009−2017, DOI: 10.1364/JOSAB.22.002009.
(56) Tan, H. S.; Piletic, I. R.; Fayer, M. D. Orientational dynamics of water confined on a nanometer length scale in reverse micelles. *J. Chem. Phys.* **2005**, *122*, No. 174501, DOI: 10.1063/1.1883605.
(57) Barbour, L. W.; Hegadorn, M.; Asbury, J. B. Microscopic inhomogeneity and ultrafast orientational motion in an organic photovoltaic bulk heterojunction thin film studied with 2D IR vibrational spectroscopy. *J. Phys. Chem. B* **2006**, *110*, 24281−24286.
(58) Valentine, M. L.; Yin, G.; Oppenheim, J. J.; Dinca, M.; Xiong, W. Ultrafast Water H-Bond Rearrangement in a Metal-Organic Framework Probed by Femtosecond Time-Resolved Infrared Spectroscopy. *J. Am. Chem. Soc.* **2023**, *145*, 11482−11487, DOI: 10.1021/jacs.3c01728.
(59) Gera, R.; Meloni, S. L.; Anna, J. M. Unraveling Confined Dynamics of Guests Trapped in Self-Assembled Pd(6)L(4) Nanocages by Ultrafast Mid-IR Polarization-Dependent Spectroscopy. *J. Phys. Chem. Lett.* **2019**, *10*, 413−418.
(60) Hao, H.; Ai, J.; Shi, C.; Zhou, D.; Meng, L.; Bian, H.; Fang, Y. Structural Dynamics of Short Ligands on the Surface of ZnSe Semiconductor Nanocrystals. *J. Phys. Chem. Lett.* **2022**, *13*, 3158−3164.
(61) Kramer, P. L.; Giammanco, C. H.; Fayer, M. D. Dynamics of water, methanol, and ethanol in a room temperature ionic liquid. *J. Chem. Phys.* **2015**, *142*, No. 212408, DOI: 10.1063/1.4914156.
(62) Fica-Contreras, S. M.; Charnay, A. P.; Pan, J.; Fayer, M. D. Rethinking Vibrational Stark Spectroscopy: Peak Shifts, Line Widths, and the Role of Non-Stark Solvent Coupling. *J. Phys. Chem. B* **2023**, *127*, 717−731.
(63) Bian, H.; Zhao, W.; Zheng, J. Intermolecular vibrational energy exchange directly probed with ultrafast two dimensional infrared spectroscopy. *J. Chem. Phys.* **2009**, *131*, No. 124501, DOI: 10.1063/1.3212618.
(64) Bondi, A. van der Waals Volumes and Radii. *J. Phys. Chem. A* **1964**, *68*, 441−451.
(65) Nyburg, S. C.; Faerman, C. H. A revision of van der Waals atomic radii for molecular crystals: N, O, F, S, Cl, Se, Br and I bonded to carbon. *Acta Crystallogr., Sect. B: Struct. Sci.* **1985**, *41*, 274−279.
(66) Bader, R. F. W.; Henneker, W. H.; Cade, P. E. Molecular Charge Distributions and Chemical Binding. *J. Chem. Phys.* **1967**, *46*, 3341−3363.
(67) Batsanov, S. S. Anisotropy of Atomic Van der Waals Radii in the Gas-Phase and Condensed Molecules. *Struct. Chem.* **2000**, *11*, 177−183.
(68) Choudalakis, G.; Gotsis, A. D. Free volume and mass transport in polymer nanocomposites. *Curr. Opin. Colloid Interface Sci.* **2012**, *17*, 132−140.
(69) Batsanov, S. S. On the additivity of van der Waals radii . *J. Chem. Soc., Dalton Trans.* **1998**, 1541−1546.
(70) Batsanov, S. S. Van der Waals Radii of Elements. *Inorg. Mater.* **2001**, *37*, 871−885.
(71) Batsanov, S. S. Van der Waals Radii of Hydrogen in Gas-Phase and Condensed Molecules. *Struct. Chem.* **1999**, *10*, 395−400.
(72) Kanaya, T.; Kawaguchi, T.; Kaji, K. Fast process of amorphous polystyrene below and above the glass transition temperature Tg as studied by quasielastic neutron scattering. *J. Chem. Phys.* **1996**, *104*, 3841−3850.
(73) Kanaya, T.; Tsukushi, I.; Kaji, K.; Gabrys, B.; Bennington, S.; Furuya, H. Localized picosecond-scale process in glassy poly(methyl methacrylate) far below Tg. *Phys. Rev. B* **2001**, *64*, No. 144202, DOI: 10.1103/PhysRevB.64.144202.
(74) Kenkre, V. M.; Tokmakoff, A.; Fayer, M. D. Theory of vibrational relaxation of polyatomic molecules in liquids. *J. Chem. Phys.* **1994**, *101*, 10618−10629.
(75) Schneider, S. H.; Boxer, S. G. Vibrational Stark Effects of Carbonyl Probes Applied to Reinterpret IR and Raman Data for Enzyme Inhibitors in Terms of Electric Fields at the Active Site. *J. Phys. Chem. B* **2016**, *120*, 9672−9684.
(76) Schmitz, H.; Müller-Plathe, F. Calculation of the lifetime of positronium in polymers via molecular dynamics simulations. *J. Chem. Phys.* **2000**, *112*, 1040−1045.

https://doi.org/10.1021/acs.macromol.3c02093
Macromolecules XXXX, XXX, XXX−XXX